Nucleic Acids Research, 2017 **1**
doi: 10.1093/nar/gkx789

Molecular mechanisms by which oxidative DNA damage promotes telomerase activity

Hui-Ting Lee[1], Arindam Bose[2], Chun-Ying Lee[1], Patricia L. Opresko[2] and Sua Myong[1,3,*]

[1]Thomas C. Jenkins Department of Biophysics, Johns Hopkins University, Baltimore, MD, 21218, USA, [2]Department of Environmental and Occupational Health, University of Pittsburgh Graduate School of Public Health and UPMC Hillman Cancer Center, Pittsburgh, PA 15261, USA and [3]Physics Frontier Center (Center for Physics of Living Cells), University of Illinois, 1110 W. Green St., Urbana, IL 61801, USA

Received May 11, 2017; Revised August 25, 2017; Editorial Decision August 28, 2017; Accepted September 14, 2017

ABSTRACT

Telomeres are highly susceptible to oxidative DNA damage, which if left unrepaired can lead to dysregulation of telomere length homeostasis. Here we employed single molecule FRET, single molecule pull-down and biochemical analysis to investigate how the most common oxidative DNA lesions, 8-oxoguanine (8oxoG) and thymine glycol (Tg), regulate the structural properties of telomeric DNA and telomerase extension activity. In contrast to 8oxoG which disrupts the telomeric DNA structure, Tg exhibits substantially reduced perturbation of G-quadruplex folding. As a result, 8oxoG induces high accessibility, whereas Tg retains limited accessibility, of telomeric G-quadruplex DNA to complementary single stranded DNA and to telomere binding protein POT1. Surprisingly, the Tg lesion stimulates telomerase loading and activity to a similar degree as an 8oxoG lesion. We demonstrate that this unexpected stimulation arises from Tg-induced conformational alterations and dynamics in telomeric DNA. Despite impacting structure by different mechanisms, both 8oxoG and Tg enhance telomerase binding and extension activity to the same degree, potentially contributing to oncogenesis.

INTRODUCTION

Telomeres are dynamic nucleoprotein complexes that cap the ends of chromosomes and protect chromosomes from degradation. In human cells, telomeres are composed of repeating 5′-TTAGGG sequences which extend to 4–15 kb of double stranded DNA (1,2), and ∼100–200 nucleotides of a single stranded overhang at the 3′ end (3). Specific proteins bind telomeric DNA to form the six-member shelterin complex, which protects the telomeric overhang from being inappropriately recognized by the DNA damage signaling and repair mechanisms (4,5) and regulates the length of the telomere (6,7). In particular, protection of telomeres 1 (POT1) binds the single stranded portion of telomeric DNA and plays an important role in telomere length regulation (8). Telomeres shorten with every cell division unless they are extended by telomerase, a reverse transcriptase which adds 5′-TTAGGG tandem repeats to the end of the telomere overhang (9). Many cancer and aging-related diseases are associated with telomere lengthening or shortening (10,11), which are also linked to oxidative stress and related DNA damage (12–15).

Oxidative stress results from an imbalance between the production of reactive oxygen species (ROS) and cellular antioxidant defenses, and contributes to the pathogenesis of numerous human diseases including cancer. Normal oxygen metabolism, inflammation and numerous environmental exposures including pollution, ionizing radiation, and ultraviolet light generate excess ROS in the cell (16–18). ROS damages cellular components including nucleic acid, thereby inducing DNA base lesions and strand breaks (19). Oxidative base lesions in chromosomal DNA are normally recognized and repaired by base excision repair enzymes including 8-Oxoguanine glycosylase (OGG1), Endonuclease III homolog 1 (NTH1) and Nei like DNA Glycosylase 1 (NEIL1) to maintain the integrity of the genome (20–22). Unrepaired DNA damage can induce mutations or interfere with DNA replication, leading to cancer and neurodegenerative diseases (15). Telomeres have been considered 'hot zones' for oxidative damage. The high guanine content (50%) in the telomere single strand overhang makes it susceptible to conversion to 8-oxoguanine (8oxoG), one of the most common oxidative lesions (23). Consecutive guanine sequences such as GGG found in telomeres are sites of preferential oxidation (24,25). However, while oxidative stress is associated with accelerated telomere shortening (26), the failure to remove 8oxoG in OGG1 deficient mice and yeast causes telomere lengthening (14,27). This raises the possibility that other forms of oxidative base damage may contribute to ROS-induced telomere shortening. While much focus has been on 8oxoG, ROS gener-

*To whom correspondence should be addressed. Tel: +1 410 516 5122; Email: smyong@jhu.edu

ates a myriad of DNA lesions (19). Thymine glycol (Tg) is the most common oxidative product of thymine, and contributes to 10–20% of ionizing radiation induced genomic damage (28). Thymine is also prevalent (33%) in the telomeric single strand overhang, and mice lacking NTH1 glycosylase, which removes Tg, show increased telomere fragility (29). While Tg is known to present a strong block to replicative and repair DNA polymerases (30), how this lesion affects telomere structure, shelterin binding, and telomerase activity remains largely unknown.

Evidence indicates that the single strand overhang of telomeres forms G-quadruplex (G4) both *in vitro* and *in vivo* (31–33). Formation of telomeric G4 in cells has been demonstrated by G4 antibodies and other G4 binding ligands (34–37). In G4 structure, four guanine bases are joined by Hoogsteen hydrogen bonding to form a planar guanine tetrad (or G-quartet) that can stack on each other. Earlier bulk phase biochemical studies showed that replacing guanine with 8oxoG in human telomere DNA disrupted the highly stable G4 conformation to different extents depending on the replacement positions (38). Recently, our study revealed that 8oxoG plays dual roles in telomere elongation. Incorporation of 8oxodGTP by telomerase terminates telomere elongation, but a pre-existing 8oxoG in telomeric DNA enhances telomere extension through disrupting G4 folding (39). The latter result may partly explain why telomere lengthening occurs in OGG1 deficient mice that fail to remove 8oxoG in telomeres (40). Bulk phase biochemical studies showed telomeric DNA containing a Tg can fold in G4 in Na^+ buffer (22), but how Tg impacts telomeric structural conformations and dynamics was unknown.

In this study, we demonstrate that although a Tg lesion in the telomeric overhang causes significantly less structural G4 disruption compared to an 8oxoG, it enhanced telomerase loading and activity to a similar extent as 8oxoG. We show that Tg promotes telomerase activity by altering the G4 conformational structure and dynamics in telomeric DNA, rather than by disrupting G4 folding. Therefore, we propose that while both of the common oxidative lesions, Tg and 8oxoG, can cause abnormal lengthening of telomeres, they achieve this outcome by different molecular mechanisms.

MATERIALS AND METHODS

DNA oligonucleotides and labeling

DNA oligonucleotides used in this study are listed in Supplementary Table S1. The single strand (ss) DNA containing 8oxoG (8oxoG4-ss) and Tg (Tg-ss) were purchased from the Midland Certified Reagent Company Inc. (Midland, TX). All other DNA oligonucleotides were purchased from IDT (Coralville, IA). All the DNA oligonucleotides were HPLC purified. 8oxoG4-ss, Tg-ss and the complementary ssDNA 18mer (Top18) had primary amine modification and were labeled with NHS-ester conjugated fluorescent dyes by following a previously established protocol (39). Briefly, DNA (40 μM) was mixed and incubated with Cy3- or Cy5-NHS ester (3mM, GE Healthcare) in 100 mM sodium bicarbonate buffer at room temperature for three hours. The excess dye was removed by performing ethanol precipitation. All the other oligonucleotides were pre-labeled or biotin conjugated by IDT. The partial duplex DNA constructs were prepared by mixing a 42-mer oligonucleotide with the 18-mer complementary oligonucleotide at a molar ratio of 1:1.2 in a buffer containing 20 mM Tris–HCl pH 7.5 and 100 mM KCl. The mixtures were incubated at 95°C for 2 min then slowly cooled to 37°C at a rate of 2°C per minute, and then cooled to room temperature at a rate of 5°C/min.

Preparation of POT1 protein and lysate from cells overexpressing human telomerase

Recombinant human POT1 protein was expressed in a baculovirus/ insect cell system and was purified as previously described (41,42). FLAG-tagged human telomerase was expressed in HEK-293T cells co-transfected with plasmids expressing hTR and FLAG-tagged hTERT in 1:3 molar ratio as previously described (7,39). Briefly, the HEK-293T cells were grown in DMEM medium with 10% FBS and 1% penicillin–streptomycin (Gibco) to 90% confluency. The cells were then transfected using Lipofectamine 2000 Reagent (Invitrogen) and allowed to grow for 48 h. The cells were harvested by trypsin detachment, washed with phosphate buffered saline (PBS) and lysed with CHAPS lysis buffer (10 mM Tris–HCl, 1 mM $MgCl_2$, 1 mM EDTA, 0.5% CHAPS, 10% glycerol, 5 mM β-mercaptoethanol, 120 U RNasin plus (Promega), 1 μg/ml each of pepstatin, aprotinin, leupeptin and chymostatin and 1 mM AEBSF) for 30 min at 4°C. The cell lysate was frozen in liquid nitrogen and stored at –80°C.

Single-molecule FRET

All single-molecule FRET (smFRET) experiments were performed using a home-built prism-type total internal reflection fluorescence (TIRF) microscope at room temperature (23 ± 1°C). The quartz slides and glass coverslips used in all the experiments were prepared by following a PEG mediated surface passivation protocol (39). Briefly, both the quartz slides and coverslips were washed with methanol and acetone, etched by sonication in 1 M KOH for 30 min, and flamed for 30 s to remove all source of fluorescence. Then the slides were treated with aminosilane for 20 minutes and coated with a mixture of 97% mPEG (m-PEG-5000, Laysan Bio, Inc.) and 3% biotin PEG (biotin-PEG-5000, Laysan Bio, Inc).

Partial duplex DNA was immobilized on the PEG coated slide via biotin-neutravidin interaction in 10 mM Tris pH7.5 and 100 mM KCl as previously described (39). An oxygen scavenging system (0.5% glucose, 10 mM 6-hydroxy-2,5,7,8-tetramethylchromane-2-carboxylic (Trolox), and 1 mg/ml glucose oxidase and 4 μg/ml catalase) was added to the imaging buffer to minimize photobleaching of fluorophores. A solid-state 532 nm laser was used to generate an evanescent field of illumination for smFRET detection of DNA samples. Data was recorded with a time resolution of 100 ms and was analyzed by Matlab. Each FRET histogram was generated from approximately 20 independent images containing 250–350 individual molecules per image, (i.e. 5000–6000 molecules are used in one histogram). The donor-leakage was corrected and each normalized histogram was fitted to Gaussian distributions with

unrestrained peak center position using Origin 2016. The reported Gaussian fitting results were obtained by averaging two to three trials, each containing over 6000 molecules. The uncertainty was expressed in the form of standard deviation calculated from multiple trials. The molecule counts were generated by incorporating over 600 individual molecules taken from two or more independent trials.

C4 probe and POT1 binding assay

Both the C4 and POT1 binding assays were carried out in the following way. A flow chamber was prepared by attaching a small plastic reservoir at one hole and a thin silicone tubing to the other hole. After immobilizing the FRET labelled DNA, 100 ul of C4 (10 nM) or POT1 (100 nM) was loaded into the reservoir. A pump equipped with a 1 ml standard disposable plastic syringe (Pump 11 Elite, Harvard Apparatus, MA) was used to draw the C4 or POT1 containing solution through the silicone tubing at a rate of 20 ul/s. Real-time FRET images were collected during and after sample injection at a frame rate of 100 or 150 ms. FRET histograms were processed in the same manner as described above. The binding kinetics for C4 and POT1 reactions were analysed by obtaining the binding time (from the moment of flow to the moment of FRET decrease). In the case of multiple steps of FRET decrease corresponding to more than one POT1 binding, only the first binding event was used to calculate the binding rate because previous work showed that the binding of the second POT1 to G4 DNA is insensitive to secondary structure (39).

Single molecule pull-down of telomerase and colocalization assay

Mouse monoclonal IgM against hTERT (LS-B95) was purchased from LifeSpan Biosciences. The antibody storage buffer was exchanged with PBS buffer by using a Bio-Gel P6 column (Bio-Rad) to remove sodium azide which could interfere with the subsequent labeling reaction with Alexa-647 dye. For labelling, the antibody was incubated with Alexa-647 C5 maleimide (Thermo Fisher) at a 1:35 molar ratio in PBS and 100 mM sodium bicarbonate on ice for 1 h. Excess dye was removed by Bio-Gel P6 column in Tris buffer. The labeled hTERT antibody was then stored in 0.02% sodium azide and 10 mM Tris–HCl, pH 7.5 at -20°C. The single molecule pull-down (SiMPull) surface was prepared by applying biotinylated mouse anti-FLAG monoclonal antibody M2 at 1:100 dilution (F9291, Sigma) and incubating for 10 min. The cell lysate containing over expressed human telomerase (1:10 dilution) was added to the antibody coated surface and incubated for 20 min. Subsequently, Cy3 labelled partial duplex DNA (10 nM, no-biotin) was applied for testing telomerase binding. The Alexa-647 conjugated mouse monoclonal antibody against hTERT (1:5000 dilution) was added to visualize the location of hTERT on the surface. Therefore, the colocalization of Cy3 and Cy5 signal indicates the telomeric DNA bound to telomerase on the surface. All the steps were carried out in telomerase reaction buffer (TRB) containing 50 mM Tris–HCl, pH 8, 50 mM KCl and 1 mM $MgCl_2$. The imaging buffer was supplemented with the same oxygen scavenging system as described above.

The alternative laser experiment was performed by using an automatic laser shutter controller synchronized with the camera such that excitation of green (Cy3-labeled DNA) and red (Alex 647-labeled antibody) can be applied in an alternating manner. Each recorded movie contains 45 frames captured at 568 nm (red) laser excitation followed by 10 frames of no excitation and 45 frames of 532 nm (green) laser excitation. The movies were analyzed by a MatLab script that averages the red signal (5–35 frames) and the green signal (60–90 frames). More than 15 000 single molecule traces obtained from three or more experiments were used for analysis of each DNA construct.

Single molecule binding and dissociation assay

Following the SiMPull experimental protocol described above, the appearance of Cy3 signals that occurred after Cy3-DNA injection was interpreted as DNA binding to the immobilized telomerase as detailed below. The binding rate was measured by measuring the time between the moment of Cy3-DNA flow into the chamber and the moment of Cy3 appearance on the surface. Dissociation experiments were performed by flowing through 100 ul of imaging buffer and measuring the time it takes for Cy3 signal to disappear from surface. For both binding and dissociation experiments, a series of short (2 s) movies were recorded sequentially from over 20 areas, rather than continuous imaging of one field of view to minimize photobleaching-induced disappearance of Cy3 and to maximize capturing molecules spread out on the imaging surface. The number of Cy3 molecules were tabulated over time to calculate the binding and dissociation rate. All the binding curves were normalized to that obtained for G3. Two or more repeats of each binding and dissociation experiment were combined to generate the binding and dissociation plot.

Telomerase extension assay

The telomerase extension assay was slightly modified from the previous protocol (7,43). *In vitro* reactions (20 μl) with oligonucleotide primers (1 μM) contained telomerase reaction buffer, 0.3 μM of 3000 Ci/mmol ^{32}P-α-dGTP (Perkin Elmer), and a cellular dNTP (Invitrogen) concentration mix of 37 μM dTTP, 24μM dATP, 29 μM dCTP and 5.2 μM dGTP. Reactions were started by adding 6.0 μl of immunopurified telomerase slurry, incubated for 1 hr at 30°C, and then terminated by adding 2 μl of 0.5 μM EDTA and heat inactivation for 20 min 65°C. A 36-mer radio end-labeled oligonucleotide was added as a loading control (LC) (8.0 fmol) to the inactivated reactions prior to purification with an Illustra MicroSpin G-25 column (GE Healthcare). Radiolabeling of LC was performed in a 20 μl reaction containing 10 pmol oligonucleotide, 1× Optikinase reaction buffer (Affymetrix), 2 μl of 3000 Ci/mmol ^{32}P-γ-ATP (Perkin Elmer) and 10 U Optikinase (Affymetrix), and incubated for 60 min at 37°C followed by heat inactivation at 65°C for 20 min. An equal volume of loading buffer (94% formamide, 0.1× Tris–borate–EDTA [TBE], 0.1% bromophenol blue, 0.1% xylene cyanol) was added to the reaction eluent from the G-25 spin column. The samples were heat denatured for 10 min at 100°C and loaded onto a 10%

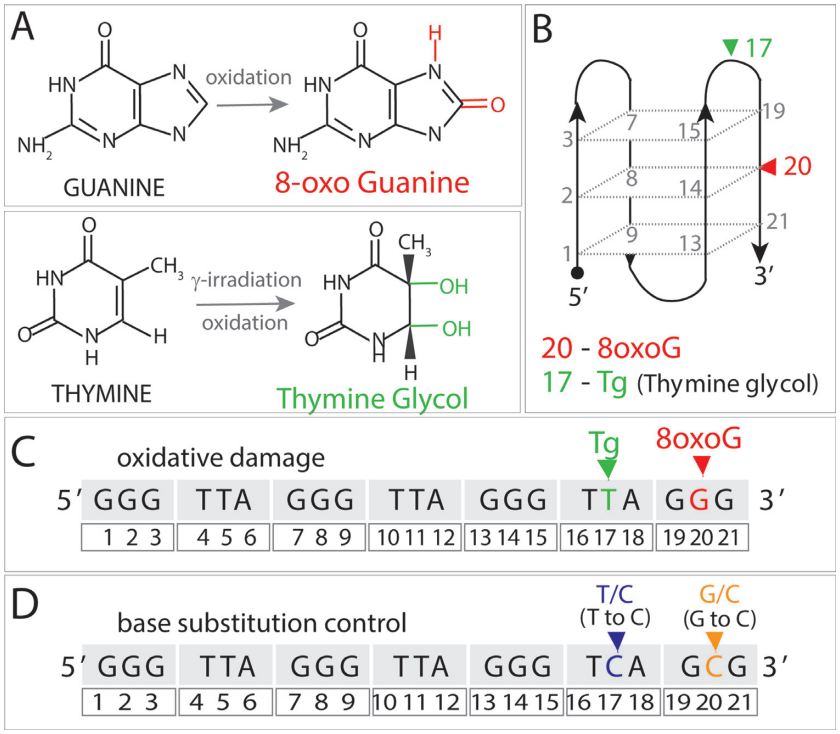

Figure 1. DNA construct design. (**A**) Chemical structure of 8-oxo-guanine (8oxoG) and Thymine Glycol (Tg). (**B**) Positions of 8oxoG and Tg in telomeric G4. (**C**, **D**) Sequence of telomeric G4 with oxidative lesions (C) and base substitutions (D).

denaturing acrylamide gel (7 M urea, 1× TBE) and electrophoresed for 70 min at constant 38 W. Samples were imaged using a Typhoon phosphorimager (GE Healthcare). Relative telomerase activity was quantitated using ImageQuant and normalized to the loading control as described previously (43,44).

RESULTS

8oxoG and Tg in telomeric DNA disrupt G-quadruplex formation to a different extent

To investigate whether a Tg lesion in telomeric DNA has a similar G4 destabilizing effect as 8oxoG, we designed a series of human telomeric sequences containing site-specific DNA lesions or base substitution mutations as controls. All DNA constructs share the same 18 base pair (bp) duplex stem and a 24 nucleotide (nt) 3′ single stranded overhang $(TTAGGG)_4$. A single 8oxoG or Tg was inserted at the fourth TTAGGG repeat (i.e. positions 20 and 17), respectively (Figure 1A–C and Supplementary Table S1). The 8oxoG at the center of the three guanines disrupts the central G-tetrad and severely reduces the thermal stability of G4 formed by $(TTAGGG)_4$ sequence (38,39). The Tg lesion is located at the 3′ thymine in the last TTAGGG repeat. As a control, we prepared G to C and T to C mutations at the same positions as the 8oxoG and Tg, respectively (Figure 1D). We carried out experiments simultaneously with each substrate for side-by-side comparisons.

The formation of G4 was monitored by fluorescence resonance energy transfer (FRET) as before (45–50). Each DNA sample has two fluorescent dyes, Cy3 at the 3′ end of the single stranded DNA and Cy5 at the 5′ end of the complementary strand of the duplex stem, such that G4 folding yields high FRET (Figure 2A–C). The FRET signal is expected to decrease with structural disruption or unfolding of the compact structure. The FRET histogram of unmodified $(TTAGGG)_4$ DNA (4R) in 100 mM KCl showed a high FRET peak centered at 0.85 (Figure 2D, top) which is consistent with the well-studied stable G4 structure (48). The histogram of the 8oxoG construct showed a dominant (83 ± 7% of the area under the Gaussian fit) mid-FRET peak at 0.53 with a smaller peak (21 ± 7%) at ∼0.8 FRET as reported earlier (39). Strikingly, the mid FRET peak of the 8oxoG construct is comparable to that of a poly-thymine overhang with a similar length of 25 nucleotides (Supplementary Figure S1), which indicates that a single 8oxoG lesion disrupts G4 formation to an unfolded structure resembling a random coil. Replacing the G with a C (G/C mutant) at the same position as 8oxoG, induced a less dramatic FRET shift to 0.65 (Figure 2D, third panel), suggesting the G to C mutation causes less G4 disruption than the 8oxoG. On the other hand, a Tg lesion in the G4 construct yields a major FRET peak (53 ± 3%) at 0.8 that extends to a shoulder at 0.73 (22 ± 9%), and a smaller broad peak at ∼0.5 FRET (30 ± 5%). This moderate shift of FRET peak indicates that only a small fraction of molecules are unfolded and that the majority of molecules have a folded but slightly less compact conformation than the 4R construct lacking lesions (0.73 and 0.8 FRET for Tg versus 0.85 for 4R). Replacing T with C (T/C mutant) at the same position as Tg does not change the value of the high FRET peak at ∼0.85 (54 ± 2% of the area), reflecting a negligible change in G4

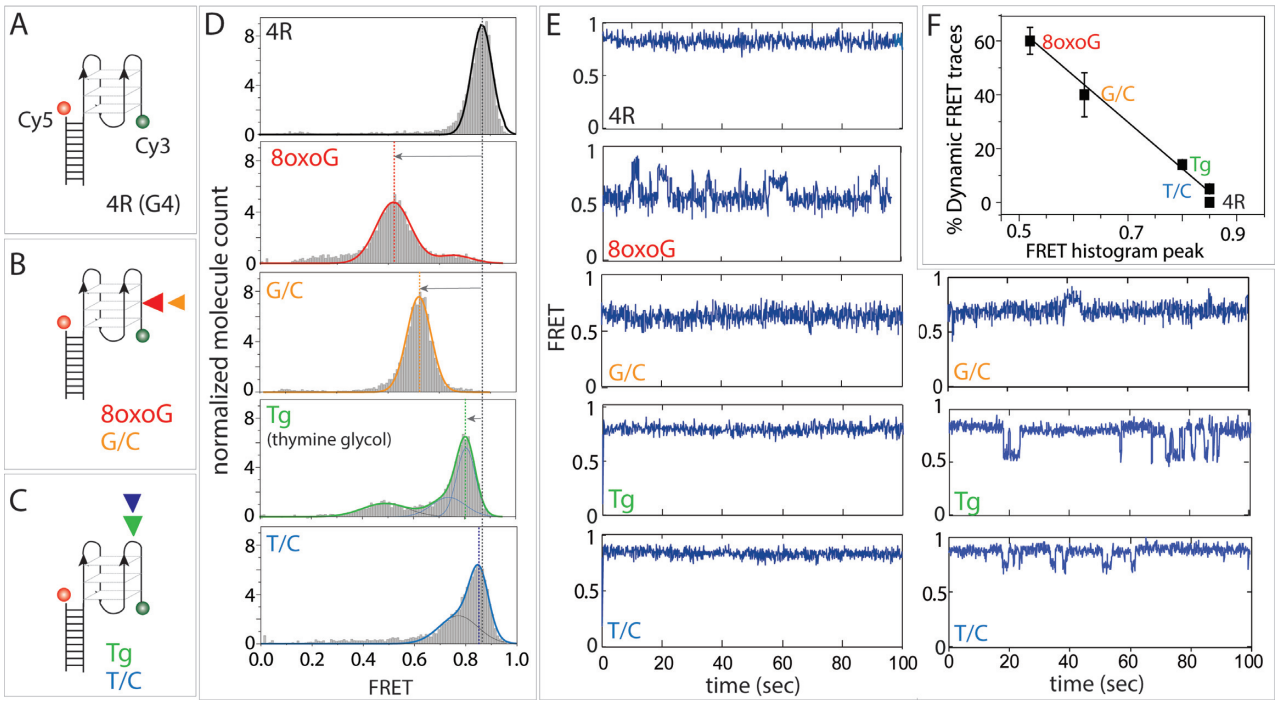

Figure 2. 8oxoG, but not Tg, disrupts telomeric G4 structure. (A–C) DNA constructs for telomeric G4 (**A**), G4 with 8oxoG or G/C mutation (**B**) and G4 with Tg or T/C mutation (**C**). (**D**) FRET histogram of each DNA construct. (**E**) Single molecule FRET traces for each DNA construct. (**F**) Plot of the percent of single molecule traces displaying dynamic FRET versus the center peak value from the FRET histograms. Error bars represent the standard deviation between trials.

folded state, compared to the wild type telomeric construct (4R). The FRET histogram of the T/C mutant construct also has a 0.75 shoulder (46 ± 2%).

Real-time single molecule FRET (smFRET) traces of constructs containing each lesion and the corresponding mutant controls were examined to gain insight into the conformational dynamics. The 4R DNA displays a steady high FRET value (Figure 2E, top), consistent with the sharp high FRET peak (Figure 2D, top). In contrast, and consistent with previous reports (39), 60 ± 5% of the 8oxoG construct traces exhibit FRET fluctuations oscillating between 0.5 and 0.8 whereas 26 ± 7% and 14 ± 11% of the traces show static 0.5 and 0.8 FRET values, respectively (Figure 2E, second row). This diverse behavior indicates that 8oxoG DNA fails to form a stable G4 but undergoes structural dynamics including occasional folding into the compact G4-like conformation indicated by the small population of high FRET molecules. The unstable nature of 8oxoG containing G4 likely arises from loss of a critical hydrogen bond in Hoogsteen base pairing and steric hindrance caused by the additional oxygen at the C8 position of guanine (51). Replacing the same guanine with cytosine (G/C) created a moderate destabilization effect with 65 ± 7% at steady high FRET and 40±8% fluctuating, which suggests that the steric hindrance, rather than loss of hydrogen bonding may be a more dominant source of disruption in the 8oxoG constructs. The disruptive effect of 8oxoG is not strictly position dependent as moving the 8oxoG and G to C mutation to the same position in the second TTAGGG repeat resulted in comparable destabilization of G4 (Supplementary Figure S2).

The smFRET traces of the Tg construct differed in composition from those obtained for constructs harboring the guanine lesion or mutation (Figure 2E, fourth row). While 64% of the Tg construct traces showed steady high FRET (0.8–0.75), 12% showed steady 0.68–0.74 FRET, 13% yielded mid-FRET at 0.5, and only 12% fluctuated between 0.8 and 0.5 FRET. The difference between the smFRET trace count and FRET histogram fitting is due to the continuous distribution of molecules having FRET values between 0.7 and 0.8. The variation of FRET above 0.65 is difficult to analyze for this construct. These traces might reflect differently folded G4 conformations (52), which will be discussed in a later section. We consider all these molecules as folded G4. Overall, 75 ± 7% of the molecules show steady FRET above 0.6, which is consistent with summing the areas under the 0.8 FRET peak and 0.73 FRET shoulder in the histogram (75 ± 9%). Similarly, summing molecules that show steady 0.5 FRET and fluctuating FRET traces (25 ± 7%) is consistent with the ∼0.5 FRET broad peak that represents 30 ± 5% of the histogram. Tg can still disrupt the G4 structure to a small degree, despite its localization within the G4 loop sequence outside of the G-tetrad. In contrast, the T to C mutant (T/C) control shows no G4 disruption. The traces obtained for the T/C mutant construct display substantially reduced dynamics and a dominant pattern (57 ± 3%) of steady high FRET (0.85–0.9), similar to the wild type construct (4R). The histogram also reveals a population (35 ± 4%) of 0.68–0.79 FRET corresponding to a 'shoulder', which we classify as differently folded G4 conformations (Figure 2). Although studies have shown that a loop sequence can influence the conformation and dynam-

ics of G4 (46), and thymine glycol disrupts the double helix in duplex DNA through its nonplanar chemical structure and steric clash (53,54). Our studies provide novel evidence that Tg can alter the G4 properties. We asked if the extent of dynamic behavior is related to the center value of the FRET peak in the histogram, which indicates the overall compactness of the G4 structure. To address this, we plotted the percentage of molecules that showed dynamic behavior (e.g. one or more FRET transition) against the center FRET value of the main peak in the histogram. This yielded a linear inverse-correlation (Figure 2F), indicating that both parameters (dynamic FRET and low FRET peak) reflect the destabilization of G4 caused by oxidative lesions or mutations.

Telomeric G4 containing a Tg lesion exhibits limited accessibility unlike G4 with 8oxoG

Next, we measured the accessibility of telomeric G4 with a Tg lesion, compared to 8oxoG, by applying an excess concentration (10nM) of the C4 probe. The oligonucleotide sequence of C4 is $(CCCTAA)_4$, which is fully complementary to the $(TTAGGG)_4$ overhang (Figure 3A) (48,55). FRET histograms collected before (gray) and after C4 injection (lime green) show the newly emerged low FRET peak that results from annealing between the two strands, which increases the distance between the Cy3 and Cy5 dyes (Figure 3B). The percentage of annealed molecules was calculated from the area of under the low FRET peak divided by the total area.

The histogram for the unmodified G4 construct (4R) did not show any shift in FRET peak upon C4 addition in 100 mM KCl. This is consistent with our earlier report, which showed that telomeric G4 is inaccessible to complementary DNA (48). In contrast, C4 addition to the 8oxoG and G/C mutant constructs completely shifted the peaks to low FRET, indicating 100% accessibility, as shown previously for 8oxoG (39). Both 8oxoG and the C/G mutation likely induce unstable and less compact conformations. Consistent with this, the FRET peak value of ∼0.5 matches that of an unfolded poly-thymine (T25, Supplementary Figure S1A). As a control, we performed annealing experiments with the poly-thymine DNA, which showed comparable accessibility to its complementary poly-adenine A25 probe (Supplementary Figure S1B). In contrast to 8oxoG, the Tg construct showed a FRET histogram that was only partially shifted by the C4 probe. The high FRET (0.8) peak was slightly reduced (∼9%) while the mid FRET (0.5) peak completely disappeared and a low FRET (0.15) peak emerged (20% of total). This result indicates that for the telomeric construct with Tg, most of the unfolded mid FRET molecules and a small fraction of high FRET molecules are accessible to the C4 probe.

For kinetic analysis, we calculated the binding rate of C4 to each DNA construct based on real-time smFRET traces. The dwell time between C4 addition and the subsequent decline of FRET was defined as the binding time of each molecule (Figure 3C). The time required for 50% of the molecules to anneal to C4 was defined as the half-time ($t_{1/2}$) and was used to compare the binding rates (Figure 3D and Supplementary Table S2). The binding rate of C4 to the 8oxoG construct was lower than that of A25 binding to the T25 single strand control. This difference indicates that even the most destabilized telomeric G4 containing an 8oxoG still maintains a structure, which makes it slightly less accessible than a fully unfolded ssDNA. Despite different accessibility, both the 8oxoG and Tg constructs exhibit the same binding rate ($t_{1/2}$ of ∼35 s), which is higher than the rate for the G/C mutant construct ($t_{1/2}$ of ∼68 s). This result implies that the loose structure formed in some Tg molecules (mid FRET) behaves similar to the 8oxoG construct, whereas the compact structure formed by a majority of Tg molecules (high FRET) has similar stability as the unmodified G4.

Telomeric G4 containing a Tg shows greatly reduced POT1 binding compared to G4 with 8oxoG

POT1 is a member of the shelterin protein complex which protects and maintains the telomeric single stranded overhang through forming protein-DNA interactions. Among the identified shelterin proteins, POT1 is the only one that binds the single stranded portion of telomeric DNA with high sequence specificity (8,41,56). Recent evidence shows the association of POT1 or POT1/TPP1 (telomere protection protein 1) complex with telomeric ssDNA can be diminished by stable G4 structure (57,58). Therefore, we tested whether the structural instability induced by 8oxoG (the majority of molecules) and Tg (a small fraction of the molecules) can enhance POT1 binding. We applied 100 nM POT1 to the same set of dye labeled telomeric G4 variant constructs. Similar to the case of C4 annealing, POT1 binding to G4 is expected to result in decreased FRET (Figure 4A).

We employed the same methods used to test C4 accessibility for the analysis of POT1 binding. The FRET histograms before (gray) and after POT1 addition (orange) shows that POT1 binding induced a FRET decrease to 0.3–0.4, in agreement with our earlier studies (47,48). The resulting FRET value is higher than that obtained for C4 binding, likely due to the structure of POT1-bound DNA displaying a sharp kink in ssDNA, which bends the long axis by ∼90° (41). The fraction of POT1 bound molecules is lower than what we reported earlier (48) due to the higher KCl concentration (100 mM) used for preparing the DNA substrates and for the experiments in this study. In this condition, ∼20% of the 4R (21± 8%) and T/C loop mutant (23 ± 2%) constructs are occupied by POT1 whereas 100% of the 8oxoG and G/C mutant constructs, and 31±5% of the Tg construct are accessible to POT1. Overall, the percentage of accessible molecules to POT1 exhibits a similar trend as the C4 probe. This result implies that the same population of unstructured molecules induced by the lesions or mutations, are accessible to both C4 and POT1.

As before, the binding rate of POT1 was calculated from the dwell time between the moment of POT1 flow and the decline of FRET to 0.3–0.4 in the smFRET traces (Figure 4C). The binding rate of POT1 is generally faster than the rate for C4 under our experimental conditions (Figure 4D). Unlike the case with C4, the POT1 binding rate followed the same trend as the binding ratio (i.e 8oxoG and G/C mutant constructs yielded the highest binding rate ($t_{1/2}$ of ∼5 s) and

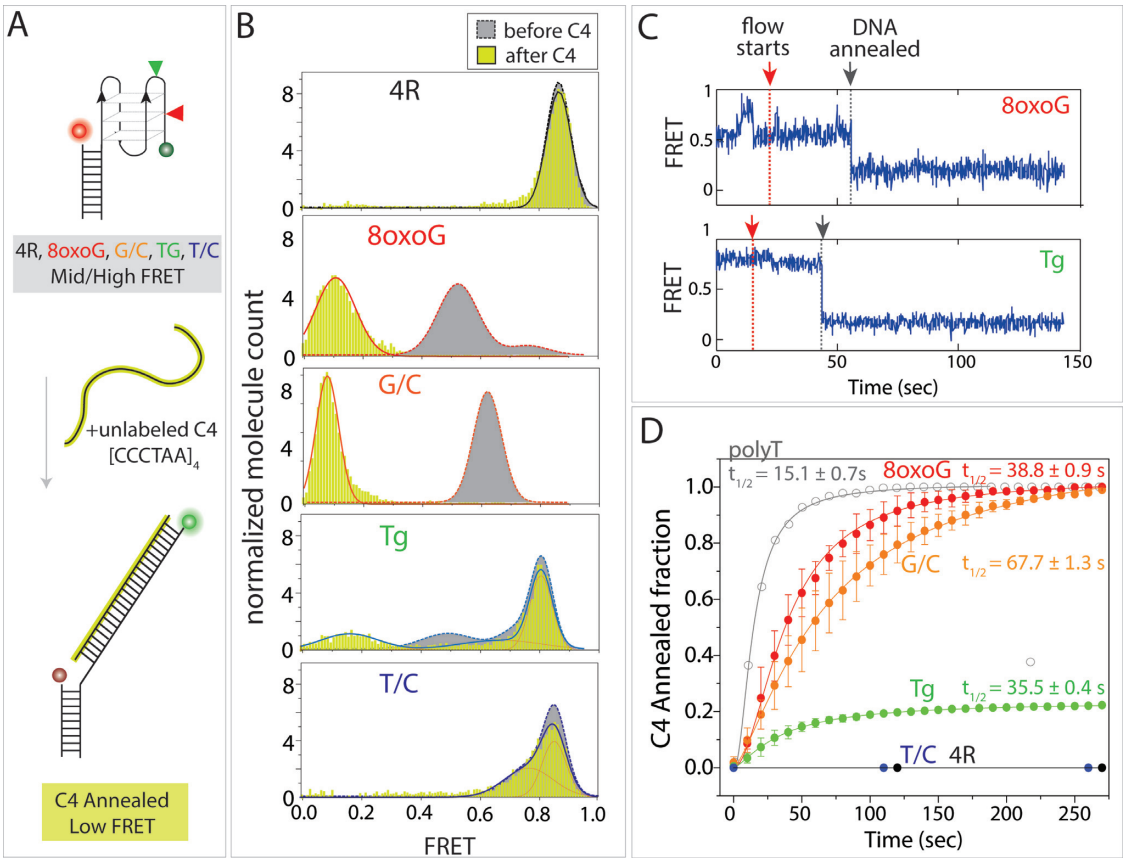

Figure 3. Tg reduces accessibility to telomeric G4 compared to 8oxoG. (**A**) Study design for testing telomeric G4 accessibility to a complementary C4 oligonucleotide (10 nM). High FRET is expected to convert to low FRET upon annealing. (**B**) FRET histogram before (gray) and after (lime green) C4 addition. (**C**) Single molecule traces displaying the moment of C4 flow and FRET decrease due to C4 annealing. (**D**) Kinetic analysis of annealing rate for all the DNA constructs tested. Error bars represent the standard deviation between trials.

the highest bound fraction (near 1)). On the other hand, the Tg DNA has binding ratios and rates higher than the 4R and T/C loop mutant constructs but much lower than the 8oxoG and G/C mutant constructs. In general, both C4 and POT1 binding data are consistent with the reduced degree of structural G4 disruption caused by Tg, compared to 8oxoG (Figure 2). Taken together, the accessibility correlates with the extent of structural destabilization caused by the lesion or mutation. In light of the finding that POT1 binding to telomeric DNA can block lesion repair (59), the enhanced POT1 binding in 8oxoG and Tg containing constructs may extend the life time of the damaged bases in telomeres.

Tg greatly increases telomerase binding and activity similar to 8oxoG in telomeric G4

The 8oxoG lesion can be bypassed during DNA synthesis, which may result in G to T mutations (23,60,61). On the other hand, Tg inhibits most DNA synthesis as many DNA polymerases stop or stall upon encountering a Tg on the template strand (30,53,62). We recently reported that a single 8oxoG lesion in human telomere sequence can restore telomerase activity through disruption of the telomeric G4 (39). Therefore, we asked whether Tg would enhance telomerase activity through alterations in G4 structure or block telomerase as observed for other polymerases. We tested the binding and activity of telomerase by using FLAG-tagged telomerase overexpressed in human HEK 293T cells (7,43,63).

We first tested the binding affinity of G4 DNA constructs to telomerase using a single molecule pull-down (64) and colocalization assay (48). The FLAG-tagged human telomerase was pulled down from cell lysate to a single molecule imaging surface coated with anti-FLAG antibody. Cy3 labeled DNA constructs were individually added to this surface, followed by Alexa 647 labeled telomerase antibody (Figure 5A). The specificity of telomerase pull-down and its interaction with the labeled telomerase antibody was tested and confirmed by omitting either FLAG antibody or cell lysate (Figure 5B). Telomerase-DNA interactions were probed by colocalization of red and green signal by alternative laser illumination in which red and green lasers excite Alexa 647 on the telomerase antibody and Cy3 on the DNA, respectively. A single molecule trace displaying a red and green signal in succession is defined as a colocalized complex, whereas a trace with only Alexa 647 signal is interpreted as unbound telomerase (Figure 5C).

Next, we tested telomerase extension activity on all G4 variant constructs by an *in vitro* telomerase extension assay (39) in which the same batch of overexpressed telomerase

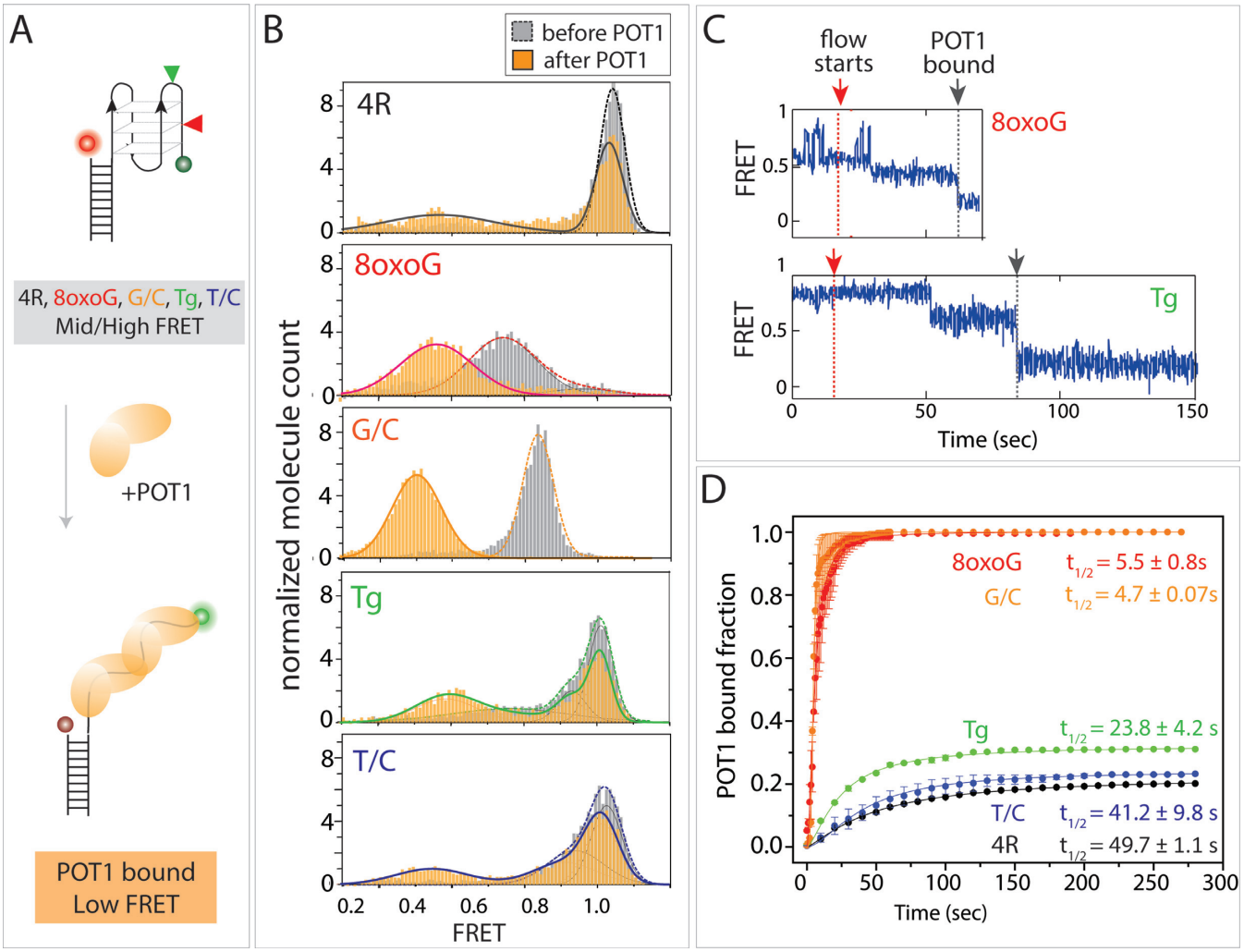

Figure 4. POT1 binding to telomeric G4 is enhanced by 8oxoG, but not significantly by Tg. (**A**) Study design for testing telomeric G4 accessibility to POT1 protein (100 nM). High FRET is expected to convert to low FRET upon POT1 association. (**B**) FRET histogram before (gray) and after (orange) POT1 addition. (**C**) Single molecule traces displaying the moment of C4 flow and FRET decrease due to POT1 binding. (D) Kinetic analysis of POT1 binding for all the DNA constructs tested. Error bars represent the standard deviation between trials.

was used for extension reactions and the products were visualized as radioactive bands on an electrophoresis gel (Figure 5D). The sum of the product bands was quantified and normalized to the loading control for each lane. For comparison, the telomerase binding (Figure 5C) and telomerase activity (Figure 5D) results were plotted side by side (Figure 5E). The G3 construct consists of $(TTAGGG)_3$ and serves as an unfolded control (39). The unmodified G4 construct (4R) exhibited the lowest telomerase binding and activity, which is consistent with our earlier report (48). Surprisingly, Tg enhanced the binding of telomerase to a similar degree as 8oxoG (Figure 5E, cyan bars). This far exceeds the level expected from the minimal structural disruption (Figure 2D) and moderately low accessibility to C4 (Figure 3B) and POT1 (Figure 4B) induced by Tg. The mutant contructs (G/C and T/C) had an intermediate level of binding between the 4R and lesion containing constructs. This intermediate level can be explained by competition between unfavorable binding caused by losing a base-pair and the favorable effect of reducing the structural stability. The higher binding of telomerase to the 8oxoG and Tg constructs, than the G3 construct, can be explained by the presence of extra guanines in the longer 8oxoG and Tg constructs that form base pairs with the telomerase RNA template. In agreement with the binding results, both 8oxoG and Tg induced substantially high telomerase extension activity (Figure 5D and E). The similar trend between the two data sets, as shown by the linear correlation in Figure 5F, suggests that the rate-limiting step of telomerase extension is likely the binding of telomerase to the telomeric overhang. The high telomerase activity observed in the Tg containing G4 was unexpected from the low accessibility to C4 and POT1. This indicates that the Tg does not interfere with annealing between the telomerase RNA template and the telomeric overhang, whereas Tg distortions impede DNA polymerases, suggesting a more complicated role of Tg in telomere processes.

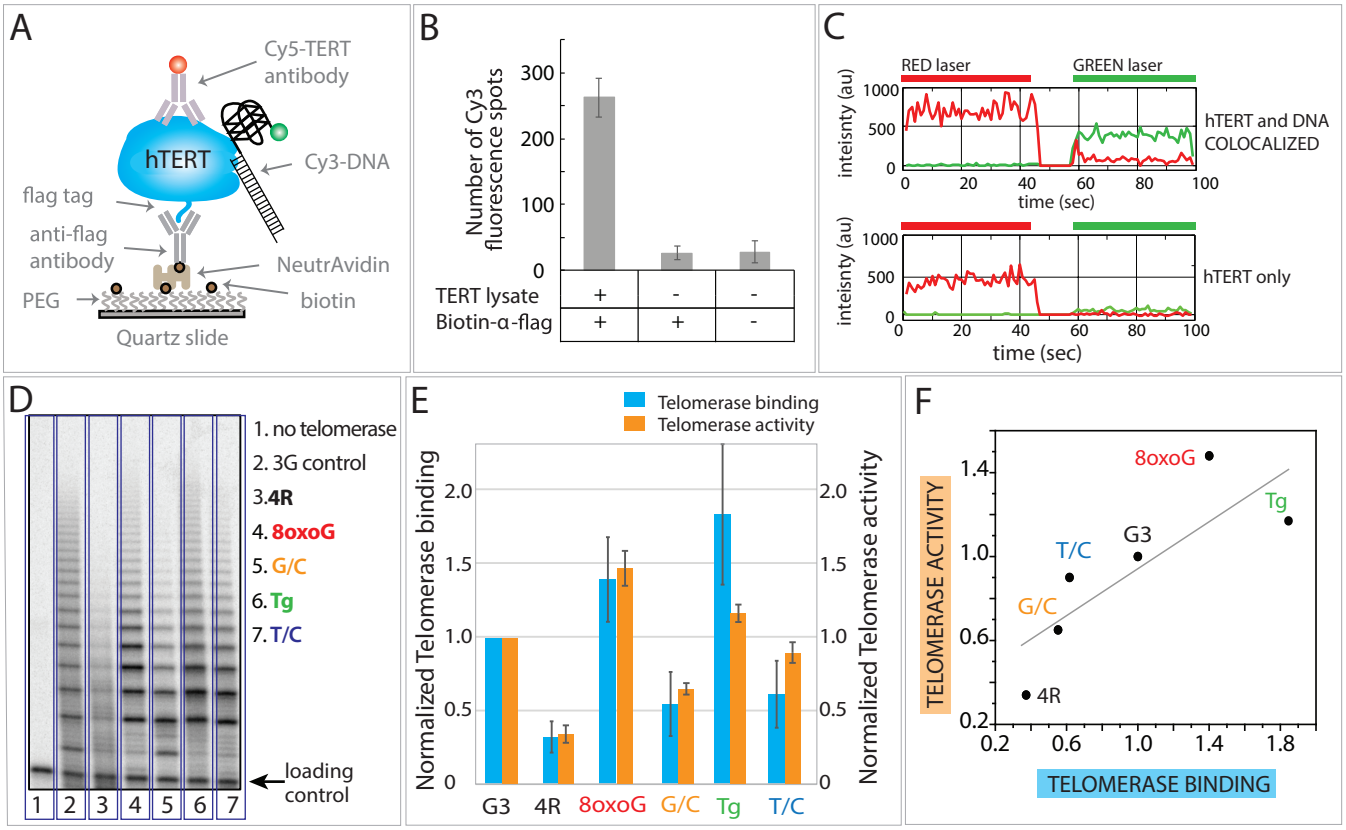

Figure 5. Tg promotes telomerase binding and activity to the same degree as 8oxoG. (**A**) Single molecule experimental platform where flag-tagged telomerase from overexpressed cell lysate was pulled down to a single molecule surface coated with anti-FLAG antibody. Cy5 labeled anti-telomerase antibody is added to visualize telomerase, and Cy3 labeled DNA is applied to this surface to measure binding affinity. (**B**) Telomerase binds specifically to the anti-FLAG surface. (**C**) Single molecule tracking of colocalized telomerase and telomeric G4 DNA. (**D**) Telomerase activity and products displayed by gel electrophoresis. (**E**) Quantified telomerase binding and activity of various G4 DNA constructs. (**F**) Plot of telomerase activity versus telomerase binding. Error bars represent the standard deviation between trials.

Tg alters the conformation and dynamics of G-quadruplex

Based on the unexpected impact of Tg on telomerase binding and activity (Figure 5), we further examined the effect of Tg on G-quadruplex folding by probing conformational dynamics. G4 formed by four repeats of the human telomeric sequence is highly polymorphic (52,65–67). The conformation and dynamics of G4 changes drastically depending on the loop size and sequence (46). Therefore, it is possible that a single moiety of Tg in the loop sequence could change the conformation of G4. To test this effect, we employed an alternative FRET construct which allows us to distinguish between parallel and nonparallel conformers of G-quadruplex (45,46). The difference lies at the position of the Cy5 which is relocated eight base pairs away from the DNA construct used previously (Figure 6A). Unlike a single high FRET peak observed for the 4R construct previously (Figures 2D, 3B and 4B), the 4R construct in this dye arrangement produces two FRET peaks at 0.4 and 0.62 representing parallel and nonparallel G-quadruplex, respectively (Figure 6B, top) (46). The fraction of parallel vs. nonparallel differs from our previous study due to the different annealing buffer (100 mM KCl) used in the current study, instead of 50 mM NaCl in the previous one (46).

The T/C loop mutation construct showed a similar double-peak FRET histogram as the 4R construct. In contrast, the Tg lesion DNA produced a much broader FRET peak (Figure 6B, bottom). The histogram shows that the parallel fraction is reduced and the non-parallel conformers are increased. In addition, the smFRET traces display dynamics between the two FRET states, likely contributing to the broadness of the FRET peaks (Figure 6C, bottom). We quantified the fraction of parallel, nonparallel and dynamic molecules for each DNA and expressed the results in a pie chart. 78 ± 1% of the 4R molecules were in a parallel state while 15±1% were in a non-parallel form, and only 6 ± 1% showed a single transition between parallel and nonparallel states (Figure 6C, top). The T/C construct showed a very similar pattern as the 4R construct, albeit a small (3%) decrease in the ratio of parallel molecules (Figure 6C and D, middle). Strikingly, the Tg construct showed only 54 ± 10% in a parallel state, with 27 ± 5% in a non-parallel form and 19±8% exhibiting dynamics. This result clearly shows that even though Tg does not disrupt G tetrad formation (Figure 2), it shifts the conformational bias toward a nonparallel state, which has been suggested to be a weaker folded conformation than the parallel conformer in our earlier study (68). Moreover, Tg also introduces more dynamics between the two states. This result likely explains the unex-

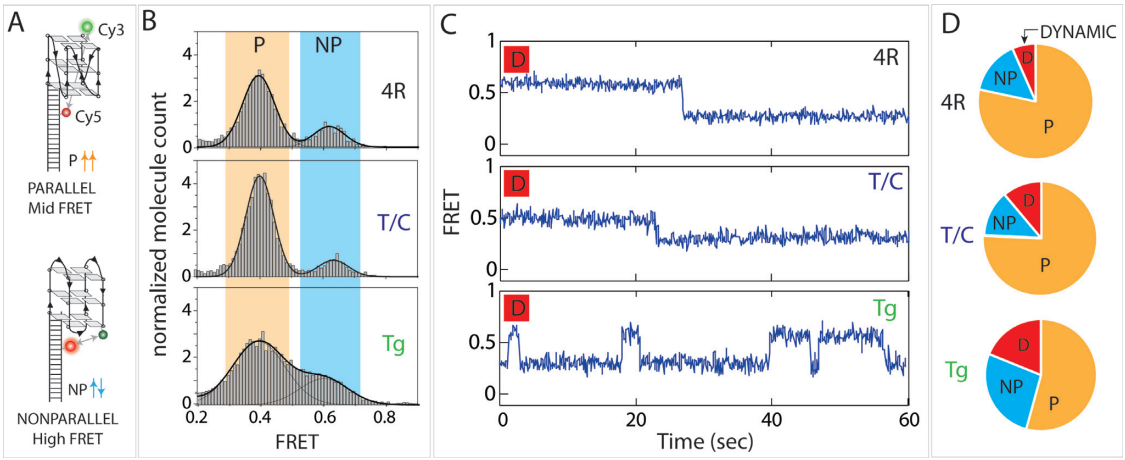

Figure 6. Tg modulates G4 conformation and dynamics. (**A**) FRET DNA constructs designed to distinguish between parallel (mid FRET) and nonparallel (high FRET). (**B**) FRET histograms of the unmodified 4R, T/C mutant and Tg lesion constructs with demarcations of parallel (orange) and nonparallel (cyan) FRET range. (**C**) Representative smFRET traces of molecules that exhibit dynamic FRET in each DNA construct. (**D**) Pie chart showing the partition of the parallel state (P, orange), nonparallel state (NP, cyan) and dynamic FRET (D, red) for the three DNA constructs.

pectedly high enhancement of telomerase binding and activity in Tg containing G4, which is indistinguishable from the enhancement level induced by 8oxoG. Despite the dynamic and non-parallel conformations, the Tg containing G4 may still act as a barrier for C4 and POT1 binding, but not for telomerase.

Telomerase prefers to bind the non-parallel forms of G-quadruplex

To test if the high telomerase binding and extension activity of the Tg construct is due to a change in binding kinetics, we measured the telomerase binding equilibrium to the Tg and 8oxoG substrates. We applied dye-labeled DNA substrates (10 nM, non-biotinylated) to a telomerase-immobilized surface (used in Figure 5) while recording the emerging fluorescent signal for 30 minutes or longer. The Tg, 8oxoG and G3 constructs all reached binding saturation within the first ten seconds while the binding of the unmodified 4R construct was substantially delayed, consistent with its low accessibility and extension activity (Supplementary Figure S3). The fractional telomerase binding for the four substrates 4R, G3, 8oxoG, and Tg is approximately 0.5, 1, 1.75, and 2, respectively, which agrees well with the colocalization binding experiment (Figure 5). We then tested the dissociation of the telomerase-bounded DNA by flowing through 100 ul of buffer. Approximately 30% of the 4R, G3 and 8oxoG substrates dissociated within the first 10 minutes and reached equilibrium without further loss up to 30 min. On the other hand, the Tg construct dissociated from telomerase at a higher rate and the dissociation continued, reaching 50% loss in 30 min (Supplementary Figure S3B). Based on these kinetic parameters, we propose that the high telomerase binding and activity observed with the Tg and 8oxoG constructs are primarily driven by the elevated binding kinetics (K_{on}) rather than the dissociation kinetics (K_{off}). In addition, the continuous dissociation observed with the Tg substrate may explain why the observed telomerase activity was lower than expected from the binding data (Figure 5E).

We asked if there is a G4 conformational preference for telomerase binding. We prepared a telomerase-bound surface and applied the 4R or Tg (nonbiotinylated) constructs with the same FRET dye locations that allows us to distinguish between the parallel and nonparallel conformers. FRET signals were recorded in real time as the DNAs bound telomerase. We collected the FRET values from the initial binding event and plotted the data into a histogram (Supplementary Figure S3C). Unlike the distribution of DNA alone (Figure 6B), which shows more parallel state (78 ± 1% of 4R and 54 ± 10% of Tg constructs), the telomerase bound DNA exhibits much less parallel conformation (24±7% of 4R and 19±3% of Tg constructs). The FRET peaks are broader than the ones in Figure 6B in part because the DNA is likely undergoing conformational dynamics as it encounters telomerase and the complementary telomerase RNA template. The inherent noise pertinent to the flow-in measurement may also contribute to peak broadening. Overall, our data demonstrate that when binding telomerase, the telomeric DNA shows a strong bias toward the nonparallel state and disfavors the parallel conformation.

DISCUSSION

Here, we report that the introduction of the common oxidative pyrimidine product, Tg, in telomeric DNA has a far less destabilizing effect on structure compared to the introduction of the common oxidative lesion 8oxoG. Correspondingly, Tg fails to promote binding of POT1 protein to telomeric G4 forming sequences, in contrast to 8oxoG which facilitates POT1 loading by disrupting the stable G4 structure. Surprisingly, we discovered that both lesions enhance telomerase binding and activity to a similar degree, but by distinctly different mechanisms, and we propose a novel mechanism by which Tg promotes telomerase activity.

A single 8oxoG unfolds G4 due to steric hindrance

Our experimental data supports earlier studies that showed an 8oxoG lesion at the central guanine disrupts the formation of G4 in human telomeric DNA, thereby enhancing telomerase activity (38,39). Here, we extended these early studies to show that the disruption caused by 8oxoG is stronger than a G to C mutation, which also lacks the essential atoms for hydrogen bonding within the guanine tetrad but does not create steric hindrance due to its smaller size. This result strengthens the generally accepted model that the disruptive ability of 8oxoG is primarily due to steric hindrance (i.e. an extra hydrogen at the N9 position repels the amine group at C2 of a guanine approaching the Hoogsteen face of 8oxoG). Disruption of G4 structure dramatically increases the overall accessibility of telomere overhangs to a complementary C-rich oligonucleotide, POT1 and telomerase loading. We also show that the binding affinity to telomerase correlates well with telomerase activity, providing a physical mechanism for the previously observed enhancement of telomerase activity on G4 substrates containing an 8oxoG(39). The elevated POT1 binding level might sequentially enhance the assembly of other shelterin proteins to further regulate telomere length or prevent glycosylases from repairing the lesion (59). The rate of POT1 binding ($t_{1/2}$ of ∼5 s) to the 8oxoG and G/C mutant substrates exceeded that of C4 binding ($t_{1/2}$ of ∼35 s) (Figures 3D and 4D). This difference might be due to the nature of POT1 binding in which both OB1 and OB2 subdomains of POT1 make highly specific interactions with the telomeric ssDNA phosphodiester group and bases (41) whereas C4 annealing involves Watson-Crick base pairing. In addition, it is plausible that the 8oxoG and G/C position may not interfere with POT1 binding, but hampers base pairing with C4. The binding specificity of POT1 might also help explain why POT1 can hardly distinguish an 8oxoG lesion from a G/C mutation.

Tg specifically enhances telomerase extension by increasing G4 conformational dynamics

By comparing with the well-studied 8oxoG as an extremely disruptive lesion, we reveal that a single Tg lesion, which is positioned outside of the guanine tetrad, also leads to significant telomere lengthening through a different molecular mechanism than the 8oxoG lesion. Based on its position, Tg located in the loop is not expected to interfere with G4 formation directly as it does not participate in the guanine tetrad formation and stacking. However, our data shows that the Tg lesion induces at least three different types of G4 alterations: (i) reduction in the tight parallel conformation, (ii) increase in the weaker non-parallel state and (iii) a greater number of molecules exhibiting dynamic behavior, transitioning between multiple states. These subtle, yet evident perturbing effects possibly arise from the configuration of glycol from Tg that disrupts the stacking of looped bases because the T/C mutation at the same position does not cause such destabilization. Although there is no structure of human telomeric DNA with a Tg lesion, existing crystal structures of telomeric G4 suggest some potential contributors for the change we observed (Supplementary Figure S4). In most telomeric G4 structures, the second thymine in the loop is involved in stacking or close contact with the neighboring guanine tetrad or other loop bases. In such a structure, the nonplanar conformation of the Tg construct makes it hard to stack with other bases. The two extra hydroxyl groups at C5 and C6 in Tg not only sterically hinders close contact but also increases the hydrophilicity of this base, resulting in more exposure to the solvent and disfavoring stable G4 conformations by deterring proper loop orientation. Moreover, this thymine base is located in the loop at the position farthest from the center of the G4 structure, which makes it the most solvent exposed, and it might adopt a different conformation when the hydrophobicity of base is altered by oxidation. A combination of these parameters, which are not mutually exclusive, may alter the G4 folding by shifting the conformational equilibrium and by increasing structural dynamics without disrupting the G4 structure (Figure 7).

Interestingly, the G4 unfolding effect induced by a Tg lesion is less significant than the pronounced effect observed with 8oxoG. While 8oxoG nearly unfolds the G4 structure (Figure 2B, second panel), Tg allows G4 to be stably maintained in folded structure (Figure 2B, fourth panel). Such subtle effects of Tg is reflected in the moderate level of C4 (Figure 3B, fourth panel) and POT1 (Figure 4B, fourth panel) binding, both of which are stimulated by partial unfolding of the G4 structure (48). The lower level of C4 and POT1 binding to the G4 containing Tg, compared to 8oxoG, suggests that Tg causes a weaker destabilization than 8oxoG. In contrast, the accessibility to telomerase was significantly enhanced by a Tg lesion (Figure 5E). This indicates that telomerase has the ability to overcome the barrier effect experienced by C4 and POT1, likely by actively invading into the weaker structure or by capturing the dynamic structure formed by the Tg containing G4. Unlike C4 and POT1, telomerase engages with telomeric DNA by pairing its internal RNA template with the telomeric overhang. In other words, the interaction entails a unique binding mode of a protein (hTERT) by assisted base pairing between RNA and DNA, which may be more efficient than the non-protein assisted annealing of C4 or the protein binding to DNA in the case of POT1. It should be noted that the improved binding of the Tg construct to telomerase was not caused by the incubation time, since incubating C4 or POT1 with the Tg DNA for 30 minutes did not increase the bound population (data not shown). Previous studies showed that telomerase could extend telomeric DNA that was folded into a bi-molecular parallel G-quadruplex (69), providing further evidence that telomerase can engage folded telomeric DNA depending on the structural conformation and properties.

The enhanced binding of telomerase to G4 containing a Tg leads to increased extension activity, which has important implications for the cellular replicative life span and tumorigenesis. Although, Nth1 deficient mice did not exhibit longer telomeres (29), unlike Ogg1 deficient mice (14), the interpretation of this result is complicated by the fact that the Nth1 glycolysis recognizes other oxidized pyrimidines including 5-hydroxycytosine and 5-hydroxyuracil (70). Therefore, these other oxidative pyrimidine lesions may interfere with telomerase if left unrepaired as well. Nevertheless, our results indicate that oxidative damage at ei-

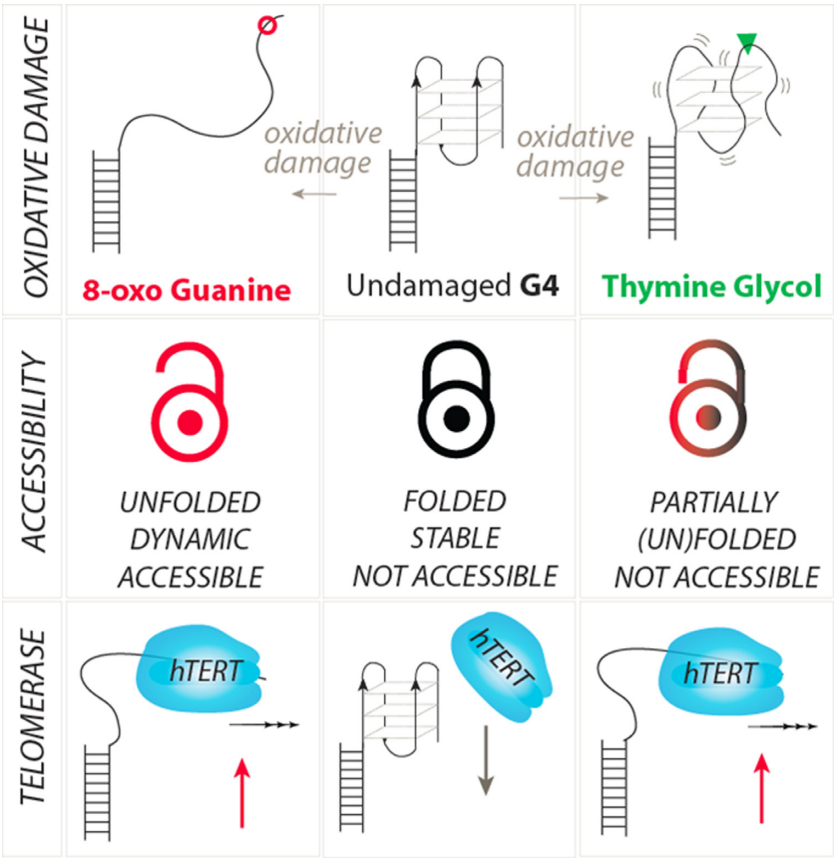

Figure 7. Summary: Effect of 8oxoG and Tg in altering telomere structure and telomerase activity. The telomeric overhang is capable of folding into a stable G-quadruplex (G4) dictated by its sequence composition of repeated 'TTAGGG'. Our study demonstrates that such folding is disrupted to different degrees based on the types and positions of DNA oxidative lesions. The 8-oxoguanine unfolds the G4 structures nearly completely whereas the thymine glycol induces less pronounced changes (i.e conformational dynamics between parallel and nonparallel G4 structures). Nevertheless, both lesions lead to substantially elevated telomerase binding and extension activity.

ther the central guanine tetrad (8oxoG) or loop (Tg) can reduce the stability of human telomeric G4 and may make the damaged telomere more accessible to proteins to varying extents. Importantly, although the structural destabilization of the Tg modification is weaker than 8oxoG, both lesions make the telomere sequence more susceptible occupation and extension by telomerase (Figure 7). Our study provides evidence for abnormal telomere elongation caused by Tg and 8oxoG lesions, which suggests a possible mechanism by which oxidative damage may promotes carcinogenesis.

SUPPLEMENTARY DATA

Supplementary Data are available at NAR Online.

ACKNOWLEDGEMENTS

The authors would like to thank Dr Ramreddy Tippana for helpful discussion about DNA construct design and Dr Helen Hwang for her help on POT1 and telomerase binding assays. We appreciate Olivia Yang's help on improving the Matlab code and in reviewing this article. We also thank Professor Taekjip Ha for his suggestion on graphic improvement.
Author contribution: The manuscript was written through contributions of S.M, H.L. and P.O. All single molecule measurement was conducted by H.L. and the telomerase extension was performed by A.B.

FUNDING

American Cancer Society [RSG-12-066-01-DMC]; National Institutes of Health [1DP2GM105453]; National Institutes of Health [GM115631]; National Institutes of Health [CA207342]; National Science Foundation Physics Frontiers Center Program [0822613] through the Center for the Physics of Living Cells (to H.T., L.C., S.M.); National Institutes of Health [ES022933 to P.L.O.]. Funding for open access charge: National Institutes of Health [NCI207342].
Conflict of interest statement. None declared.

REFERENCES

1. Dalgard,C., Benetos,A., Verhulst,S., Labat,C., Kark,J.D., Christensen,K., Kimura,M., Kyvik,K.O. and Aviv,A. (2015) Leukocyte telomere length dynamics in women and men: menopause vs age effects. *Int. J. Epidemiol.*, **44**, 1688–1695.
2. Okuda,K., Bardeguez,A., Gardner,J.P., Rodriguez,P., Ganesh,V., Kimura,M., Skurnick,J., Awad,G. and Aviv,A. (2002) Telomere length in the newborn. *Pediatr. Res.*, **52**, 377–381.
3. Cimino-Reale,G., Pascale,E., Battiloro,E., Starace,G., Verna,R. and D'Ambrosio,E. (2001) The length of telomeric G-rich strand

3′-overhang measured by oligonucleotide ligation assay. *Nucleic Acids Res.*, **29**, E35.
4. Palm,W. and de Lange,T. (2008) How shelterin protects mammalian telomeres. *Annu. Rev. Genet.*, **42**, 301–334.
5. Rodriguez,R., Muller,S., Yeoman,J.A., Trentesaux,C., Riou,J.F. and Balasubramanian,S. (2008) A novel small molecule that alters shelterin integrity and triggers a DNA-damage response at telomeres. *J. Am. Chem. Soc.*, **130**, 15758–15759.
6. Abreu,E., Aritonovska,E., Reichenbach,P., Cristofari,G., Culp,B., Terns,R.M., Lingner,J. and Terns,M.P. (2010) TIN2-tethered TPP1 recruits human telomerase to telomeres in vivo. *Mol. Cell. Biol.*, **30**, 2971–2982.
7. Hwang,H., Opresko,P. and Myong,S. (2014) Single-molecule real-time detection of telomerase extension activity. *Sci. Rep.*, **4**, 6391.
8. Baumann,P. and Cech,T.R. (2001) Pot1, the putative telomere end-binding protein in fission yeast and humans. *Science*, **292**, 1171–1175.
9. Morin,G.B. (1989) The human telomere terminal transferase enzyme is a ribonucleoprotein that synthesizes TTAGGG repeats. *Cell*, **59**, 521–529.
10. Blasco,M.A. (2005) Telomeres and human disease: ageing, cancer and beyond. *Nat. Rev. Genet.*, **6**, 611–622.
11. Zhu,X., Han,W., Xue,W., Zou,Y., Xie,C., Du,J. and Jin,G. (2016) The association between telomere length and cancer risk in population studies. *Sci. Rep.*, **6**, 22243.
12. Askree,S.H., Yehuda,T., Smolikov,S., Gurevich,R., Hawk,J., Coker,C., Krauskopf,A., Kupiec,M. and McEachern,M.J. (2004) A genome-wide screen for Saccharomyces cerevisiae deletion mutants that affect telomere length. *Proc. Natl. Acad. Sci. U.S.A.*, **101**, 8658–8663.
13. Lu,J. and Liu,Y. (2010) Deletion of Ogg1 DNA glycosylase results in telomere base damage and length alteration in yeast. *EMBO J.*, **29**, 398–409.
14. Wang,Z., Rhee,D.B., Lu,J., Bohr,C.T., Zhou,F., Vallabhaneni,H., de Souza-Pinto,N.C. and Liu,Y. (2010) Characterization of oxidative guanine damage and repair in mammalian telomeres. *PLoS Genet.*, **6**, e1000951.
15. Cooke,M.S., Evans,M.D., Dizdaroglu,M. and Lunec,J. (2003) Oxidative DNA damage: mechanisms, mutation, and disease. *FASEB J.*, **17**, 1195–1214.
16. Poljsak,B. and Fink,R. (2014) The protective role of antioxidants in the defence against ROS/RNS-mediated environmental pollution. *Oxid. Med. Cell Longev.*, **2014**, 671539.
17. Aseervatham,G.S., Sivasudha,T., Jeyadevi,R. and Arul Ananth,D. (2013) Environmental factors and unhealthy lifestyle influence oxidative stress in humans–an overview. *Environ. Sci. Pollut. Res. Int.*, **20**, 4356–4369.
18. Lonkar,P. and Dedon,P.C. (2011) Reactive species and DNA damage in chronic inflammation: reconciling chemical mechanisms and biological fates. *Int. J. Cancer*, **128**, 1999–2009.
19. Cadet,J. and Wagner,J.R. (2013) DNA base damage by reactive oxygen species, oxidizing agents, and UV radiation. *Cold Spring Harb. Perspect. Biol.*, **5**, a012559.
20. Nishioka,K., Ohtsubo,T., Oda,H., Fujiwara,T., Kang,D., Sugimachi,K. and Nakabeppu,Y. (1999) Expression and differential intracellular localization of two major forms of human 8-oxoguanine DNA glycosylase encoded by alternatively spliced OGG1 mRNAs. *Mol. Biol. Cell*, **10**, 1637–1652.
21. Dizdaroglu,M., Karahalil,B., Senturker,S., Buckley,T.J. and Roldan-Arjona,T. (1999) Excision of products of oxidative DNA base damage by human NTH1 protein. *Biochemistry*, **38**, 243–246.
22. Zhou,J., Liu,M., Fleming,A.M., Burrows,C.J. and Wallace,S.S. (2013) Neil3 and NEIL1 DNA glycosylases remove oxidative damages from quadruplex DNA and exhibit preferences for lesions in the telomeric sequence context. *J. Biol. Chem.*, **288**, 27263–27272.
23. Nishimura,S. (2006) 8-Hydroxyguanine: From its discovery in 1983 to the present status. *Proc. Jpn. Acad. Ser. B Phys. Biol. Sci.*, **82**, 127–141.
24. Kawanishi,S. and Oikawa,S. (2004) Mechanism of telomere shortening by oxidative stress. *Ann. N. Y. Acad. Sci.*, **1019**, 278–284.
25. Oikawa,S., Tada-Oikawa,S. and Kawanishi,S. (2001) Site-specific DNA damage at the GGG sequence by UVA involves acceleration of telomere shortening. *Biochemistry*, **40**, 4763–4768.
26. von Zglinicki,T., Pilger,R. and Sitte,N. (2000) Accumulation of single-strand breaks is the major cause of telomere shortening in human fibroblasts. *Free Radic. Biol. Med.*, **28**, 64–74.
27. Fouquerel,E., Parikh,D. and Opresko,P. (2016) DNA damage processing at telomeres: The ends justify the means. *DNA Repair (Amst.)*, **44**, 159–168.
28. Frenkel,K., Goldstein,M.S. and Teebor,G.W. (1981) Identification of the cis-thymine glycol moiety in chemically oxidized and gamma-irradiated deoxyribonucleic acid by high-pressure liquid chromatography analysis. *Biochemistry*, **20**, 7566–7571.
29. Vallabhaneni,H., O'Callaghan,N., Sidorova,J. and Liu,Y. (2013) Defective repair of oxidative base lesions by the DNA glycosylase Nth1 associates with multiple telomere defects. *PLoS Genet.*, **9**, e1003639.
30. McNulty,J.M., Jerkovic,B., Bolton,P.H. and Basu,A.K. (1998) Replication inhibition and miscoding properties of DNA templates containing a site-specific cis-thymine glycol or urea residue. *Chem. Res. Toxicol.*, **11**, 666–673.
31. Parkinson,G.N., Lee,M.P. and Neidle,S. (2002) Crystal structure of parallel quadruplexes from human telomeric DNA. *Nature*, **417**, 876–880.
32. Dai,J., Punchihewa,C., Ambrus,A., Chen,D., Jones,R.A. and Yang,D. (2007) Structure of the intramolecular human telomeric G-quadruplex in potassium solution: a novel adenine triple formation. *Nucleic Acids Res.*, **35**, 2440–2450.
33. Phan,A.T., Kuryavyi,V., Luu,K.N. and Patel,D.J. (2007) Structure of two intramolecular G-quadruplexes formed by natural human telomere sequences in K+ solution. *Nucleic Acids Res.*, **35**, 6517–6525.
34. Johnson,J.E., Smith,J.S., Kozak,M.L. and Johnson,F.B. (2008) In vivo veritas: using yeast to probe the biological functions of G-quadruplexes. *Biochimie*, **90**, 1250–1263.
35. Huppert,J.L. (2008) Hunting G-quadruplexes. *Biochimie*, **90**, 1140–1148.
36. Maizels,N. (2006) Dynamic roles for G4 DNA in the biology of eukaryotic cells. *Nat. Struct. Mol. Biol.*, **13**, 1055–1059.
37. Lipps,H.J. and Rhodes,D. (2009) G-quadruplex structures: in vivo evidence and function. *Trends Cell Biol.*, **19**, 414–422.
38. Vorlickova,M., Tomasko,M., Sagi,A.J., Bednarova,K. and Sagi,J. (2012) 8-oxoguanine in a quadruplex of the human telomere DNA sequence. *FEBS J.*, **279**, 29–39.
39. Fouquerel,E., Lormand,J., Bose,A., Lee,H.T., Kim,G.S., Li,J., Sobol,R.W., Freudenthal,B.D., Myong,S. and Opresko,P.L. (2016) Oxidative guanine base damage regulates human telomerase activity. *Nat. Struct. Mol. Biol.*, **23**, 1092–1100.
40. Sarkar,J. and Liu,Y. (2016) The origin of oxidized guanine resolves the puzzle of oxidation-induced telomere-length alterations. *Nat. Struct. Mol. Biol.*, **23**, 1070–1071.
41. Lei,M., Podell,E.R. and Cech,T.R. (2004) Structure of human POT1 bound to telomeric single-stranded DNA provides a model for chromosome end-protection. *Nat. Struct. Mol. Biol.*, **11**, 1223–1229.
42. Sowd,G., Lei,M. and Opresko,P.L. (2008) Mechanism and substrate specificity of telomeric protein POT1 stimulation of the Werner syndrome helicase. *Nucleic Acids Res.*, **36**, 4242–4256.
43. Latrick,C.M. and Cech,T.R. (2010) POT1-TPP1 enhances telomerase processivity by slowing primer dissociation and aiding translocation. *EMBO J.*, **29**, 924–933.
44. Zaug,A.J., Podell,E.R., Nandakumar,J. and Cech,T.R. (2010) Functional interaction between telomere protein TPP1 and telomerase. *Genes Dev.*, **24**, 613–622.
45. Tippana,R., Hwang,H., Opresko,P.L., Bohr,V.A. and Myong,S. (2016) Single-molecule imaging reveals a common mechanism shared by G-quadruplex-resolving helicases. *Proc. Natl. Acad. Sci. U.S.A.*, **113**, 8448–8453.
46. Tippana,R., Xiao,W. and Myong,S. (2014) G-quadruplex conformation and dynamics are determined by loop length and sequence. *Nucleic Acids Res.*, **42**, 8106–8114.
47. Hwang,H., Buncher,N., Opresko,P.L. and Myong,S. (2012) POT1-TPP1 regulates telomeric overhang structural dynamics. *Structure*, **20**, 1872–1880.
48. Hwang,H., Kreig,A., Calvert,J., Lormand,J., Kwon,Y., Daley,J.M., Sung,P., Opresko,P.L. and Myong,S. (2014) Telomeric overhang length determines structural dynamics and accessibility to telomerase and ALT-associated proteins. *Structure*, **22**, 842–853.

49. Hwang,H., Opresko,P. and Myong,S. (2014) Single-molecule real-time detection of telomerase extension activity. *Sci. Rep.*, **4**, 6391.
50. Lee,J.Y. and Kim,D.S. (2009) Dramatic effect of single-base mutation on the conformational dynamics of human telomeric G-quadruplex. *Nucleic Acids Res.*, **37**, 3625–3634.
51. Cheong,V.V., Heddi,B., Lech,C.J. and Phan,A.T. (2015) Xanthine and 8-oxoguanine in G-quadruplexes: formation of a G.G.X.O tetrad. *Nucleic Acids Res.*, **43**, 10506–10514.
52. Lee,J.Y., Okumus,B., Kim,D.S. and Ha,T. (2005) Extreme conformational diversity in human telomeric DNA. *Proc. Natl. Acad. Sci. U.S.A.*, **102**, 18938–18943.
53. Dolinnaya,N.G., Kubareva,E.A., Romanova,E.A., Trikin,R.M. and Oretskaya,T.S. (2013) Thymidine glycol: the effect on DNA molecular structure and enzymatic processing. *Biochimie*, **95**, 134–147.
54. Minetti,C.A., Remeta,D.P., Iden,C.R., Johnson,F., Grollman,A.P. and Breslauer,K.J. (2015) Impact of thymine glycol damage on DNA duplex energetics: Correlations with lesion-induced biochemical and structural consequences. *Biopolymers*, **103**, 491–508.
55. Zaug,A.J., Podell,E.R. and Cech,T.R. (2005) Human POT1 disrupts telomeric G-quadruplexes allowing telomerase extension in vitro. *Proc. Natl. Acad. Sci. U.S.A.*, **102**, 10864–10869.
56. Wang,F. and Lei,M. (2011) Human telomere POT1-TPP1 complex and its role in telomerase activity regulation. *Methods Mol. Biol.*, **735**, 173–187.
57. Ray,S., Bandaria,J.N., Qureshi,M.H., Yildiz,A. and Balci,H. (2014) G-quadruplex formation in telomeres enhances POT1/TPP1 protection against RPA binding. *Proc. Natl. Acad. Sci. U.S.A.*, **111**, 2990–2995.
58. Mullins,M.R., Rajavel,M., Hernandez-Sanchez,W., de la Fuente,M., Biendarra,S.M., Harris,M.E. and Taylor,D.J. (2016) POT1-TPP1 binding and unfolding of telomere DNA discriminates against structural polymorphism. *J. Mol. Biol.*, **428**, 2695–2708.
59. Theruvathu,J.A., Darwanto,A., Hsu,C.W. and Sowers,L.C. (2014) The effect of Pot1 binding on the repair of thymine analogs in a telomeric DNA sequence. *Nucleic Acids Res.*, **42**, 9063–9073.
60. Kuchino,Y., Mori,F., Kasai,H., Inoue,H., Iwai,S., Miura,K., Ohtsuka,E. and Nishimura,S. (1987) Misreading of DNA templates containing 8-hydroxydeoxyguanosine at the modified base and at adjacent residues. *Nature*, **327**, 77–79.
61. Shibutani,S., Takeshita,M. and Grollman,A.P. (1991) Insertion of specific bases during DNA synthesis past the oxidation-damaged base 8-oxodG. *Nature*, **349**, 431–434.
62. Clark,J.M. and Beardsley,G.P. (1989) Template length, sequence context, and 3′-5′ exonuclease activity modulate replicative bypass of thymine glycol lesions in vitro. *Biochemistry*, **28**, 775–779.
63. Cristofari,G. and Lingner,J. (2006) Telomere length homeostasis requires that telomerase levels are limiting. *EMBO J.*, **25**, 565–574.
64. Jain,A., Liu,R., Ramani,B., Arauz,E., Ishitsuka,Y., Ragunathan,K., Park,J., Chen,J., Xiang,Y.K. and Ha,T. (2011) Probing cellular protein complexes using single-molecule pull-down. *Nature*, **473**, 484–488.
65. Dai,J., Carver,M. and Yang,D. (2008) Polymorphism of human telomeric quadruplex structures. *Biochimie*, **90**, 1172–1183.
66. Cang,X., Sponer,J. and Cheatham,T.E. 3rd (2011) Explaining the varied glycosidic conformational, G-tract length and sequence preferences for anti-parallel G-quadruplexes. *Nucleic Acids Res.*, **39**, 4499–4512.
67. Noer,S.L., Preus,S., Gudnason,D., Aznauryan,M., Mergny,J.L. and Birkedal,V. (2016) Folding dynamics and conformational heterogeneity of human telomeric G-quadruplex structures in Na+ solutions by single molecule FRET microscopy. *Nucleic Acids Res.*, **44**, 464–471.
68. Kreig,A., Calvert,J., Sanoica,J., Cullum,E., Tipanna,R. and Myong,S. (2015) G-quadruplex formation in double strand DNA probed by NMM and CV fluorescence. *Nucleic Acids Res.*, **43**, 7961–7970.
69. Moye,A.L., Porter,K.C., Cohen,S.B., Phan,T., Zyner,K.G., Sasaki,N., Lovrecz,G.O., Beck,J.L. and Bryan,T.M. (2015) Telomeric G-quadruplexes are a substrate and site of localization for human telomerase. *Nat. Commun.*, **6**, 7643.
70. Krokan,H.E. and Bjoras,M. (2013) Base excision repair. *Cold Spring Harb. Perspect. Biol.*, **5**, a012583.